

Charging by quantum measurement

Jia-shun Yan¹ and Jun Jing^{1,*}

¹*School of Physics, Zhejiang University, Hangzhou 310027, Zhejiang, China*

(Dated: September 29, 2022)

We propose a quantum charging scheme fueled by measurements on ancillary qubits serving as disposable chargers. A stream of identical qubits are sequentially coupled to a quantum battery of $N + 1$ levels and measured by projective operations after joint unitary evolutions of optimized intervals. If qubit-chargers are prepared in excited state and measured on ground state, their excitations (energy) can be near-completely transferred to battery by iteratively updating the optimized measurement intervals. Starting from its ground state, the battery could be constantly charged to an even higher energy level. Starting from a thermal state, the battery could also achieve a near-unit rate of ergotropy and energy under $\sim N$ measurements, when a population inversion occurs. If qubit-chargers are prepared in ground state and measured on excited state, useful work extracted by measurements alone could transform the battery from a thermal state to a high-ergotropy state before the success probability vanishes. Our findings reveal novel features of quantum measurement on shaping the nonequilibrium system.

I. INTRODUCTION

Over one century, the classical batteries have driven the revolutions in personal electronics and in the automotive sector. As energy-storage units in a brand-new paradigm, quantum batteries [1–4] are expected to outperform the classical counterparts by widely exploiting the advantages based on quantum operations and promoting their efficiency under the constraint of quantum thermodynamics [5–7].

Enormous attentions were paid to charging quantum batteries, as the primary step in the charge-store-discharge cycle. Many charging protocols have been presented, including but not limited to charging by entangling operations [8, 9], charging with dissipative [10, 11], unitary, and collisional processes [12, 13], and charging collectively and in parallel [14, 15]. Many-body interactions [16–18] and energy fluctuations [19, 20] have also been explored to raise the upper-bound for charging power and capacity. In particular, local and global interactions are designed to transfer energy from various thermodynamical resources to batteries. The maximum rate and amount in energy transfer are subject to relevant timescales of evolution and relaxation.

Quantum measurements, particularly the repeated projections onto a chosen state or a multidimensional subspace, could change dramatically the transition rate of the measured system [21–23]. In quantum thermodynamics [24], direct measurements have been applied to extract energy from a hot thermal reservoir [25] or move a quantum particle against a force [26]. Quantum engineering by virtue of measurements on ancillary system, which generates a net nonunitary propagator, is capable to purify and cool down quantum systems [27–30]. In general, a projective measurement or postselection on ancillary system would herald the target system to be in a de-

sired state with a finite probability. Therefore, quantum measurements can become a useful resource more than the heat or work reservoirs, serving as fuels powering a thermodynamical or state-engineering scheme through a nonunitary procedure. In this work, we address quantum measurements in the context of charging quantum battery. It is interesting to find that the joint evolution of chargers and batteries interrupted by projections on a specific subspace of chargers could speed up the charging process and promote the amount of accumulated energy and ergotropy.

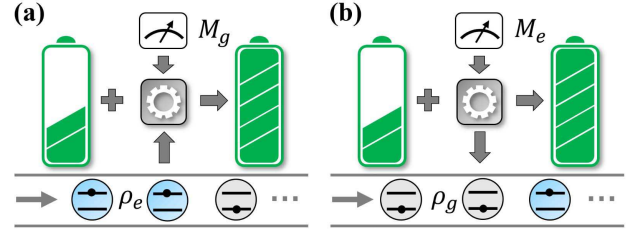


FIG. 1. (a) Power-on and (b) Power-off charging schemes. Identically prepared ancillary qubits line up to interact with the battery for a period of time. In the end of each round of joint evolution, a projective measurement is performed on the qubit to induce a nonunitary charging operation on the battery. In (a) power-on charging, qubits are initialized as the excited state ρ_e and the projection M_g is performed on its ground state. Energy gain of the battery is mainly from the qubit excitations. In (b) power-off charging, qubits are initialized as the ground state ρ_g and the projection M_e is on the excited state. Useful work extracted by measurements simultaneously charges the battery and the ancillary qubits.

In particular, we propose a charging-via-measurement scheme in a quantum collision framework [31–33]. As disposable chargers a sequence of identical qubits line up to temporarily couple to the battery (a multilevel system with a finite number of evenly spaced ladders). On the projective measurement in the end of the joint evolution, the ancillary qubit is replaced with a new one and

* Email address: jingjun@zju.edu.cn

then the scheme continues. Figures 1(a) and 1(b) show a *power-on* and a *power-off* charging schemes, respectively. When the qubits are initially in the excited state $\rho_e = |e\rangle\langle e|$, the projective measurement on the ground state $M_g = |g\rangle\langle g|$ transfers the energy of excited qubits to the battery. The energy gain for battery increases linearly with the number of measurements and the charging power is gradually enhanced as well. Full population inversion is realized when the measurement number is close to the battery size. When the qubits are prepared as the ground states $\rho_g = |g\rangle\langle g|$, still the battery can be charged by measuring the ancillary qubits on the excited state $M_e = |e\rangle\langle e|$. Useful work extracted entirely from repeated measurements simultaneously charges the battery and the qubit.

The rest of this work is structured as follows. In Sec. II, we introduce a general model of charging by measurements, whereby the charging or discharging effect is analysed in view of a general projective-measurement. In Sec. III, we present the power-on charging scheme. We find an optimized measurement interval to maximize the measurement probability, by which both energy and ergotropy of the battery scale linearly with the number of measurements. Section IV devotes to the power-off charging scheme. For both schemes, we evaluated the charging efficiency by charging power, state distribution, energy and ergotropy of the battery. In Sec. V, we summarize the whole work.

II. MODEL OF CHARGING BY GENERAL MEASUREMENTS

We aim for charging a quantum battery by performing measurements on the ancillary qubits as disposable chargers. The scheme is constructed by rounds of joint evolution and projective measurement. The full Hamiltonian

$$H = H_B + H_C + V \quad (1)$$

consists of a target battery system H_B , a sequence of identical charger qubits (only one of them is coupled to the battery in each round and the others are separable), and the interaction V between battery and the current working charger H_C . The battery is initially in a thermal state $\rho_B = e^{-\beta H_B} / \text{Tr}[e^{-\beta H_B}]$, $\beta \equiv 1/k_B T$, with finite energy yet zero ergotropy. The qubits are prepared as the same mixed state $\rho_C = q|g\rangle\langle g| + (1-q)|e\rangle\langle e|$ with a ground-state occupation $q \in [0, 1]$ before linking to the battery. In each round, the joint evolution of the battery and the working qubit is described by the time-evolution operator $U = \exp(-iH\tau)$. The period of coupling τ might be constant or varying with respect to all the rounds. An instantaneous projective measurement M on the qubit is implemented in the end of the round, and then the (unnormalized) joint state becomes

$$\rho'_{\text{tot}} = MU\rho_B \otimes \rho_C U^\dagger M \quad (2)$$

with a finite measurement probability $P = \text{Tr}[MU\rho_B \otimes \rho_C U^\dagger]$. Note $M = M^2$ for projection operators. After measurement, the charger qubit is decoupled from the battery system and withdrawn, then another qubit is loaded to the next round. The charging scheme is non-deterministic in essence and thus employs a feedback mechanism: the measurement outcome determines whether to launch the next round of charging cycle or to restart from the beginning.

In our model, a quantum battery has $N + 1$ energy ladders with Hamiltonian $H_B = \omega_b \sum_{n=0}^N n|n\rangle\langle n|$, where ω_b is the energy unit of the battery. $\hbar = k_B = 1$. The ladder operators are defined as $A^\dagger = \sum_{n=1}^N \sqrt{n}|n\rangle\langle n-1|$ and $A = \sum_{n=1}^N \sqrt{n}|n-1\rangle\langle n|$. The Hamiltonian for each charge qubit is $H_C = \omega_c |e\rangle\langle e|$, where ω_c is the energy spacing between the ground $|g\rangle$ and excited states $|e\rangle$. The battery and the qubits are coupled by the exchange interaction $V = g(\sigma_- A^\dagger + \sigma_+ A)$, where g is the coupling strength and σ_- and σ_+ denote the transition operators of the qubit. Then the full Hamiltonian in the rotating frame with respect to $H_0 = \omega_b(\sum_{n=0}^N n|n\rangle\langle n| + |e\rangle\langle e|)$ reads

$$H = \Delta |e\rangle\langle e| + g(\sigma_- A + \sigma_+ A^\dagger), \quad (3)$$

where $\Delta = \omega_c - \omega_b$ represents the energy detuning between charger qubit and battery.

The charging procedure is piecewisely concatenated by a sequence of joint evolutions of battery and charger qubits, which is interrupted by instantaneous projective measurements $M_\varphi = |\varphi\rangle\langle \varphi|$ over a particular state $|\varphi\rangle = \cos(\theta/2)|g\rangle + \sin(\theta/2)|e\rangle$, $0 \leq \theta \leq \pi$, of the working qubit. After a round of an interval τ , the battery state becomes

$$\rho_B(\tau) = \text{Tr}_C[\rho'_{\text{tot}}] = \frac{\mathcal{D} + \mathcal{C}}{P_\varphi} = \frac{\mathcal{D} + \mathcal{C}}{\text{Tr}[M_\varphi U \rho_B \otimes \rho_C U^\dagger]}, \quad (4)$$

where \mathcal{D} is the diagonal (population) part in the density matrix of the battery system without normalization and \mathcal{C} is the off-diagonal (coherence) part

$$\mathcal{C} = \frac{\sin \theta}{2} \sum_{n=1}^N \alpha_n^* [q\lambda_n p_n + (1-q)\lambda_n^* p_{n-1}] |n-1\rangle\langle n| + \text{H.c.} \quad (5)$$

Here both $\alpha_n = \cos \Omega_n \tau + i\Delta \sin(\Omega_n \tau) / 2\Omega_n$ and $\lambda_n = -ie^{-i\Delta\tau/2} g\sqrt{n} \sin(\Omega_n \tau) / \Omega_n$ are renormalization coefficients, $\Omega_n = \sqrt{g^2 n + \Delta^2 / 4}$ is the Rabi frequency, and p_n is the initial thermal occupation on the n th level of battery, i.e., $\rho_B = \sum_{n=0}^N p_n |n\rangle\langle n|$ with $p_n = [e^{-\beta\omega_b n} - e^{-\beta\omega_b(n+1)}] / [1 - e^{-\beta\omega_b(N+1)}]$.

The population part could be divided as $\mathcal{D} = \mathcal{D}_{\text{charge}} + \mathcal{D}_{\text{discharge}}$ due to the heating or cooling contribution on the battery system from various positive operator-valued

measures (POVM). By Eqs. (2) and (4), we have

$$\begin{aligned}\mathcal{D}_{\text{charge}} &= (1-q)\cos^2\frac{\theta}{2}\mathcal{M}_{eg}[\rho_B] + q\sin^2\frac{\theta}{2}\mathcal{M}_{ge}[\rho_B], \\ \mathcal{D}_{\text{discharge}} &= q\cos^2\frac{\theta}{2}\mathcal{M}_{gg}[\rho_B] + (1-q)\sin^2\frac{\theta}{2}\mathcal{M}_{ee}[\rho_B],\end{aligned}\quad (6)$$

where $\mathcal{M}_{ij}[\cdot] \equiv R_{ij} \cdot R_{ij}^\dagger$, $i, j \in \{e, g\}$, represents the j th element of the i th POVM, satisfying the normalization condition of Kraus operators $\sum_j R_{ij}^\dagger R_{ij} = I_B$. In particular, $R_{ij} \equiv \langle j|U|i\rangle$ is the Kraus operator acting on the state space of the battery, where i and j label respectively the initial state and the measured state of the ancillary qubit. It is straightforward to find that

$$\begin{aligned}\mathcal{M}_{eg}[\rho_B] &= \sum_{n=1}^N |\lambda_n(\tau)|^2 p_{n-1} |n\rangle\langle n|, \\ \mathcal{M}_{ge}[\rho_B] &= \sum_{n=0}^{N-1} |\lambda_{n+1}(\tau)|^2 p_{n+1} |n\rangle\langle n|, \\ \mathcal{M}_{gg}[\rho_B] &= \sum_{n=0}^N |\alpha_n(\tau)|^2 p_n |n\rangle\langle n|, \\ \mathcal{M}_{ee}[\rho_B] &= \sum_{n=0}^{N-1} |\alpha_{n+1}(\tau)|^2 p_n |n\rangle\langle n|.\end{aligned}\quad (7)$$

According to Naimark's dilation theorem [34], a set of projective measurements $\{M_j\}$ acting on one of the subspaces \mathcal{H}_1 of the total space $\mathcal{H}_{\text{tot}} = \mathcal{H}_1 \otimes \mathcal{H}_2$ could induce a POVM on another subspace \mathcal{H}_2 with a map $\mathcal{H}_2 \rightarrow \mathcal{H}_{\text{tot}}$. In our context, an arbitrary projective measurement $M_\varphi = |\varphi\rangle\langle\varphi|$ defined in the space of the charger qubit induces a POVM $\mathcal{M}_{\cdot,\varphi}[\rho_B]$ acting on the battery. And the map is constructed by $U|i\rangle$ with the joint unitary evolution U , according to the initial state of the charger $|i\rangle$. Therefore, as shown in Eq. (7), we have two sets of POVM in the bare basis of the charger qubit: $\mathcal{M}_{e,j \in \{e,g\}}$ and $\mathcal{M}_{g,j \in \{e,g\}}$. For instance, \mathcal{M}_{eg} represents a POVM on the battery induced by projection on the ground state of the qubit that is initially in the excited state.

$\mathcal{D}_{\text{charge}}$ in Eq. (6) is a linear combination of \mathcal{M}_{eg} and \mathcal{M}_{ge} in Eq. (7). The former replaces a smaller p_n with a larger $|\lambda_n|^2 p_{n-1}$ (under a proper choice of τ) for all the excited states. On the contrary, the latter moves the populations on higher levels to lower levels, which could also enhance the battery energy through a significant renormalization (Note the largest population p_0 on the ground level has been eliminated) over the population distribution. In contrast, $\mathcal{D}_{\text{discharge}}$ is a linear combination of \mathcal{M}_{gg} and \mathcal{M}_{ee} . Both of them reduce the populations of the excited state due to the fact that $|\alpha_{n>0}| \leq |\alpha_0| = 1$ and then enhance the comparative weight of the ground-state population. Then they are inclined to discharge the battery. The dependence of the charging or discharging effects on the choices of initial and measured states is justified in Fig. 2 by the ratio between the average population after a single round of evolution-and-measurement and the initial thermal average population

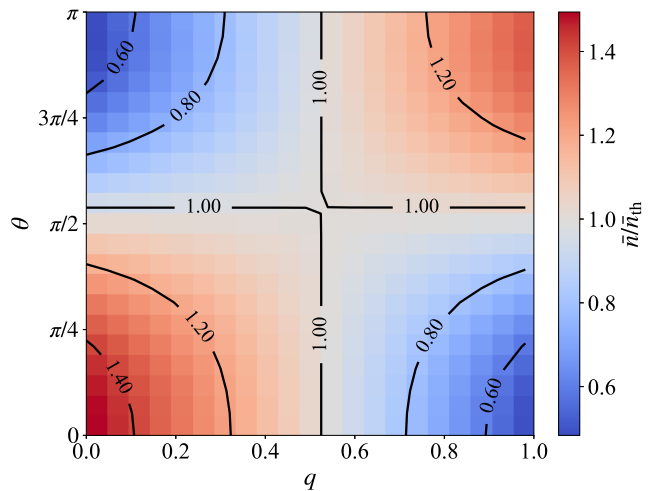


FIG. 2. Ratio $\bar{n}/\bar{n}_{\text{th}}$ between the average population \bar{n} of the battery after a single measurement and the initial thermal population $\bar{n}_{\text{th}} \equiv \text{Tr}[\bar{n}\rho_B]$ in the space of θ and q . The size of battery is $N = 100$, the initial inverse temperature is $\beta = 0.1/\omega_c$, and the measurement interval is $\tau = 8/\omega_c$.

in the parametric space of θ and q , describing respectively the weights of the measured state and the initial state of qubit on the ground state. The two blue-diagonal corners in Fig. 2 correspond to the POVMs \mathcal{M}_{gg} and \mathcal{M}_{ee} that could be used to cool down the target system. For instance, the lower right corner \mathcal{M}_{gg} with $q = 1$ and $\theta = 0$ describes the mechanism of cooling-by-measurement in the resonator system [29]. More important to the current work, the lower left corner \mathcal{M}_{eg} with $q = 0$ and $\theta = 0$ and the upper right corner \mathcal{M}_{ge} with $q = 1$ and $\theta = \pi$ motivate our investigation on the following power-on and power-off charging schemes, respectively. Here it is found that the former scheme is more efficient than the latter in terms of the rate $\bar{n}/\bar{n}_{\text{th}}$ with certain measurement interval.

III. POWER-ON CHARGING

In this section, we present the power-on charging scheme described by \mathcal{M}_{eg} in which the charger qubits are prepared in their excited states with $q = 0$ and the projective measurement is performed on the ground state with $\theta = 0$. Then the density matrix of the battery after $m \geq 1$ rounds of measurements reads

$$\rho_{\text{on}}^{(m)} = \frac{\mathcal{M}_{eg}[\rho_{\text{on}}^{(m-1)}]}{P_g(m)} = \frac{\sum_{n=m}^N |\lambda_n(\tau)|^2 p_{n-1}^{(m-1)} |n\rangle\langle n|}{P_g(m)} \quad (8)$$

where $\rho_{\text{on}}^{(m-1)} = \sum_{n=m-1}^N p_n^{(m-1)} |n\rangle\langle n|$ represents the battery state with population $p_n^{(m-1)}$ on the state $|n\rangle$ after $(m-1)$ rounds of measurements under the power-on charging scheme. $p_n^{(0)} = p_n$ is the initial thermal

occupation and $\rho_{\text{on}}^{(0)} = \rho_B$. The normalization coefficient $P_g(m) = \sum_{n=m}^N |\lambda_n(\tau)|^2 p_{n-1}^{(m-1)}$ is the measurement probability of the m th round. In Eq. (8), a projective measurement generates a population transfer between neighboring energy ladders of the battery $p_n^{(m)} \leftarrow |\lambda_n(\tau)|^2 p_{n-1}^{(m-1)}$ with an n -dependent weight $|\lambda_n(\tau)|^2$. The battery is initially set as a Gibbs thermal state where populations follow an exponential decay function with the occupied-state index n . Thus it is charged step by step by the POVM \mathcal{M}_{eg} , which moves the populations of lower-energy states up to higher-energy states. And the normalization coefficient $|\lambda_n(\tau)|^2$ ranging from zero to unit is τ -dependent. $p_n^{(m)}$ is thus determined by the measurement interval τ between two consecutive measurements. With a sequence of properly designed or optimized measurement intervals, the battery could be constantly charged by the projection-induced POVM.

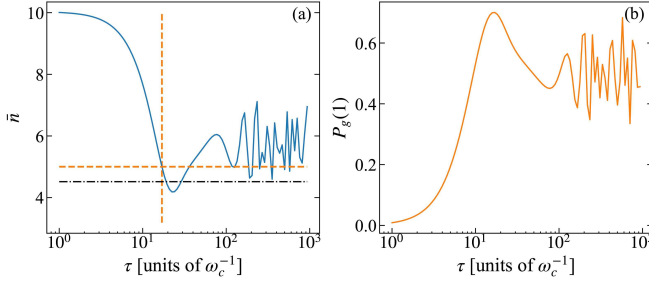


FIG. 3. (a) Average population and (b) Measurement probability as functions of measurement interval τ after a single measurement within the power-on scheme. The black dot-dashed line denotes the initial thermal occupation \bar{n}_{th} of the battery. In (a) the two crossing orange dashed lines locate the average population after a single measurement with a maximal measurement probability obtained from (b). The updated \bar{n} is found to be larger than \bar{n}_{th} in magnitude, that ensures a success charging with a significant probability. The battery size is $N = 100$, the initial inverse temperature is $\beta = 0.2/\omega_c$, the detuning between charger qubit and battery is $\Delta/\omega_c = 0.02$, and the coupling strength is $g/\omega_c = 0.04$.

In Fig. 3(a), the average population \bar{n} after one measurement is plotted as a function of measurement interval τ . The initial thermal population \bar{n}_{th} is plotted for comparison (see the black dot-dashed line). One can find that a considerable charging effect appears in a range of measurement interval when $\tau \leq 20/\omega_c$. Over this critical point, a cooling-effect range appears where the average population is less than the initial population. And then \bar{n} fluctuates with an even larger τ . To pursue the highest charging power, it is intuitively that one should choose a measurement interval as small as possible. It is however under the constraint of a practical coupling strength between charger qubits and battery. In addition, if the measurement interval is smaller than one eigen-period of the charger qubit ($\tau \sim 1/\omega_c$ or less), the joint-evolution time would be too short to detect the charger qubit (initially in the excited state) in its ground state. That would

extremely suppress the measurement probability.

As shown in Fig. 3(b), the measurement probability $P_g(1)$ approaches zero when $\tau\omega_c \rightarrow 0$. When increasing the measurement interval to about $\tau\omega_c = 17$, we can observe that $P_g(1)$ climbs to a peak value over 70% and then declines with τ and ends up with a random fluctuation. It is interesting and important to find that there is a mismatch between the discharging range of \bar{n} in Fig. 3(a) and the peak value of $P_g(1)$. In Fig. 3(a), two crossing orange dashed lines locate the optimized measurement interval for the maximized $P_g(1)$ in Fig. 3(b). On that point it is found that a single measurement on the charger qubit could enhance the battery energy from about $4.5\omega_b$ to $5.0\omega_b$. Then it is expected that the battery would be constantly charged with a significant probability if the measurement intervals for the ensued rounds of evolution-and-measurement can be optimized by maximizing the measurement probability. In the mean time, the charger qubit that is prepared as the excited state and measured on the ground state has achieved the maximum efficiency with respect to the energy transfer during each charging round.

The measurement probability can be written by a finite summation involving sine functions $P_g(m) = \sum_{n=m}^N \sin^2(\Omega_n \tau) p_{n-1}^{(m-1)}$ with $\Omega_n \approx g\sqrt{n}$ under the resonant or near-resonant condition. It is estimated that for a sufficiently large N and a sufficiently short τ ,

$$\begin{aligned}
 P_g(m) &= \sum_{n=m}^N [1 - \cos^2(\Omega_n \tau)] p_{n-1}^{(m-1)} \\
 &\approx \sum_n p_{n-1}^{(m-1)} - \sum_n \cos^2(\Omega_n \tau) p_{n-1}^{(m-1)} \quad (9) \\
 &= 1 - \left[1 - \left(\Omega_{\bar{n}+1}^{(m-1)} \tau \right)^2 + \dots \right] \\
 &\approx 1 - \cos^2(\Omega_{\bar{n}+1} \tau),
 \end{aligned}$$

where $\Omega_{\bar{n}+1}^{(m-1)} = g\sqrt{\bar{n}^{(m-1)} + 1}$ is the average Rabi frequency under the resonant condition and $\bar{n}^{(m-1)} \equiv \sum_n (n-1) p_{n-1}^{(m-1)}$ is the average population for the battery after $(m-1)$ rounds of measurements. The optimized measurement interval is thus given by an iterative formula:

$$\tau_{\text{opt}}^{(m)} = \frac{\pi}{2\Omega_{\bar{n}+1}^{(m-1)}}. \quad (10)$$

It means that τ_{opt} is updated by the battery's average population of the last round. Note the leading-order correction from a nonvanishing detuning Δ is in its second order.

Equation (10) can be justified under various temperatures and during a full sequence of rounds for a charging process. The optimized measurement interval is inversely proportional to the square root of the average population that is inversely proportional to β . In Fig. 4(a), one can find that the overall behaviors of $P_g(1)$ with various β are similar to that in Fig. 3(b). A larger β yields a larger τ_{opt}

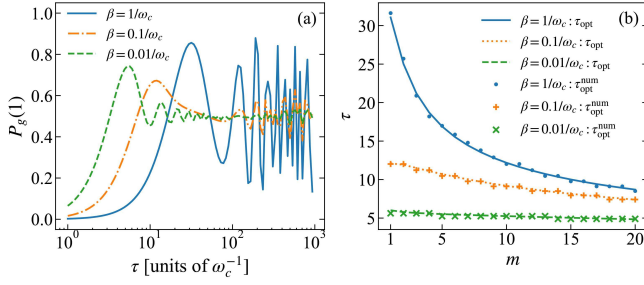


FIG. 4. (a) Measurement probability as a function of measurement interval under various temperatures. (b) Sequences of the optimized measurement intervals under various temperatures, where τ_{opt} is analytically obtained by Eq. (10) and $\tau_{\text{opt}}^{\text{num}}$ represents the numerical result. The other parameters are the same as those in Fig. 3.

to have a peak value of $P_g(1)$. In another word, one has to perform more frequent measurements to charge a battery initially with a higher temperature. It is also reflected in Fig. 4(b), by which we compare the analytical results through Eq. (10) and the numerical results of optimized measurement intervals for 20 rounds of measurements under various temperatures. It is found that for β across three orders in magnitude, the analytical formula (10) is well suited to obtain the maximized measurement probability that represents the maximum energy input from the charger qubits. The effective temperature of battery increases during the charging process. Then τ_{opt} gradually decreases with m . It is consistent with the fact that coupling a qubit to a higher temperature battery with uniform energy spacing between ladders induces a faster transition between the excited state and the ground state of the qubit.

In terms of the charging efficiency, we have two remarks in our scheme on measurement. First, a decreasing τ_{opt} with m could give rise to an increasing charging power

$$\mathcal{P}(m) \equiv \frac{\text{Tr} \left[H_B \left(\rho_{\text{on}}^{(m)} - \rho_{\text{on}}^{(m-1)} \right) \right]}{\tau_{\text{opt}}^{(m)}}, \quad (11)$$

which describes the amount of energy deposited per unit time in a charging round. It is found that such a battery would be charged faster and faster during the first stage of charging process. Second, Fig. 4(b) indicates that for the time-varying optimized intervals, dramatic changes appear in the first several rounds and then they become almost invariant as the measurements are implemented. It holds back the time-scales between neighboring projection operations from being too small to lose experimental feasibility.

According to Eq. (8), the average population of the battery after m measurements under the resonant or near-resonant condition is

$$\bar{n}^{(m)} = \frac{\sum_{n=m}^N n \sin^2(\Omega_n \tau) p_{n-1}^{(m-1)}}{\sum_{n=m}^N \sin^2(\Omega_n \tau) p_{n-1}^{(m-1)}}. \quad (12)$$

Around $n' = \bar{n}^{(m-1)} + 1$, we have

$$\sin^2(\Omega_n \tau) = \sin^2(\Omega_{n'} \tau) + \frac{g\tau \sin^2(2\Omega_{n'} \tau)}{2\sqrt{n'}}(n - n') + \dots \quad (13)$$

All of these sine functions could be approximated to the second order of $(n - n')$ as $\sin^2 \Omega_n \tau \approx \sin^2 \Omega_{\bar{n}+1}^{(m-1)} \tau_{\text{opt}}^{(m)} = 1$ when each measurement is implemented with the optimal time in Eq. (10). Therefore, Eq. (12) could be expressed with the average population of last charging round $\bar{n}^{(m-1)}$:

$$\begin{aligned} \bar{n}^{(m)} &\approx \frac{\sum_{n=m}^N (n-1) p_{n-1}^{(m-1)} + \sum_{n=m}^N p_{n-1}^{(m-1)}}{\sum_{n=m}^N p_{n-1}^{(m-1)}} \\ &\approx \bar{n}^{(m-1)} + 1. \end{aligned} \quad (14)$$

It is assumed that after a number of measurements, $\sum_{n=m}^N p_{n-1}^{(m-1)} \approx 1$. This result indicates that the battery gain a unit of energy in each round of evolution-and-measurement. In another word, POVM \mathcal{M}_{eg} promotes a near-perfect energy transfer from charger qubits to battery, whose charging efficiency then overwhelms the charging scheme without measurements [13].

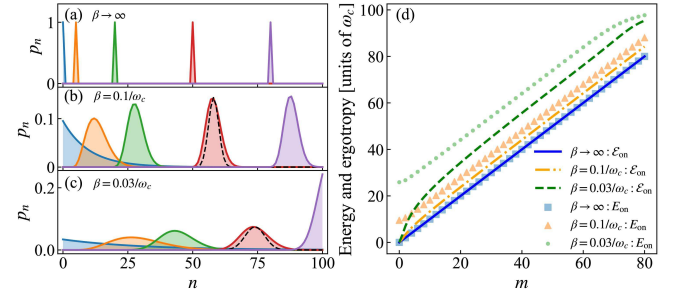


FIG. 5. Population distributions of the battery after $m = 0$ (blue), $m = 5$ (orange), $m = 20$ (green), $m = 50$ (red), and $m = 80$ (purple) measurements for various initial temperatures: (a) $\beta \rightarrow \infty$, (b) $\beta = 0.1/\omega_c$, and (c) $\beta = 0.03/\omega_c$ under the power-on charging scheme. In (b) and (c), the black-dashed curves describe the Gaussian distributions with the same average population and variance of the battery state after $m = 50$ measurements under finite temperatures. In (d), battery ergotropy and energy under various temperatures are plotted respectively with lines and markers. The other parameters are the same as those in Fig. 3.

Consider the simplest case $\rho_B = |0\rangle\langle 0|$, where the battery is prepared in its ground state or zero-temperature state as described by the blue distribution in Fig. 5(a). Each round of POVM \mathcal{M}_{eg} induced by projective measurement allows a full state transfer from lower to higher levels $p_{n+1}^{(m)} \leftarrow p_n^{(m-1)}$. After $m < N$ measurements, the whole population is transferred to the m th energy ladder of the battery with zero variance

$$\Delta n^{(m)} \equiv \sum_n n^2 p_n^{(m)} - \left[\bar{n}^{(m)} \right]^2 = 0. \quad (15)$$

And in this case, the charged energy

$$E_{\text{on}}^{(m)} \equiv \text{Tr}[H_B \rho_{\text{on}}^{(m)}] \quad (16)$$

and the ergotropy

$$\mathcal{E}_{\text{on}}^{(m)} \equiv E_{\text{on}}^{(m)} - \text{Tr}[\sigma_{\text{on}}^{(m)} H_B] \quad (17)$$

are exactly the same in magnitude. Here $\sigma_{\text{on}}^{(m)}$ is the passive state obtained by realigning the populations of $\rho_{\text{on}}^{(m)}$ in decreasing order, which has none extractable energy under cyclic unitary operations [35]. The power-on charging scheme then realizes a full conversion between excitations of charger qubits and usable energy of the battery when the latter starts from a pure Fock state.

In Fig. 5(b), the battery is prepared with a moderate temperature. It is gradually transformed from a thermal distributed state to a Gaussian-like distributed one, whose mean value increases with rounds of measurements. For the battery state after $m = 50$ measurements, a Gaussian state ρ_G is distinguished by a black dashed curve, whose average population and variance are chosen the same as those for $\rho_{\text{on}}^{(m)}$. The fidelity $F(m) = \text{Tr}[\sqrt{\sqrt{\rho_G} \rho_{\text{on}}^{(m)}} \sqrt{\rho_G}]$ between them is found to be 0.82 when $m = 50$. Analogous to the Fano factor [36], we can also use the ratio of the variance and the mean value $f(m) \equiv \Delta n^{(m)} / \bar{n}^{(m)}$ to measure the evolution of these Gaussian-like distributions. It is found that $f(5) = 1.37$, $f(20) = 0.33$, $f(50) = 0.13$, and $f(80) = 0.08$. As measurements are constantly implemented, the battery state distribution thus becomes even sharper and the populations tend to concentrate around \bar{n} , allowing more extractable energy.

The varying distributions under a higher temperature are provided in Fig. 5(c), where the fidelity $F(m = 50)$ is still about 0.82 and the variance is much extended in Fock states. Comparing the purple distributions in Figs. 5(c) and 5(b), a population inversion occurs in the state space of the higher-temperature battery more quickly than the lower-temperature one, as the measurement number is close to the battery size $m \sim N$.

We demonstrate the energy and ergotropy of the battery as functions of the measurement number in Fig. 5(d). It is interesting to find that the finite-temperature batteries under our power-on scheme could also achieve a near-unit rate of ergotropy and energy as the zero-temperature battery, which has been popularly considered in previous schemes of quantum battery. Both energy and ergotropy increase in a nearly linear way as Eq. (14) with implementations of POVMs. Before the occurrence of population inversion, the comparative amount of the unusable energy for a lower-temperature battery is larger than a higher-temperature one, e.g., when $m = 60$, we have $\mathcal{E}_{\text{on}}^{(m)} / E_{\text{on}}^{(m)} \approx 0.94$ for $\beta = 0.1/\omega_c$ and $\mathcal{E}_{\text{on}}^{(m)} / E_{\text{on}}^{(m)} \approx 0.91$ for $\beta = 0.03/\omega_c$. In contrast, when $m = 80$, we have $\mathcal{E}_{\text{on}}^{(m)} / E_{\text{on}}^{(m)} \approx 0.96$ and 0.98 , for $\beta = 0.1/\omega_c$ and $0.03/\omega_c$, respectively. It is reasonable since population inversion

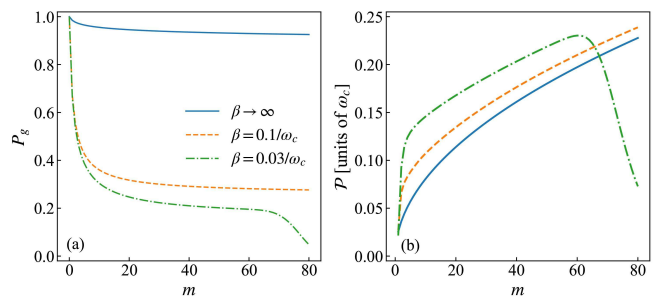


FIG. 6. (a) Success probability and (b) Charging power under power-on charging as functions of measurement number. All parameters are the same as Fig. 3 except the inverse temperature.

indicates a close-to-unit utilization rate of ergotropy and energy.

The success probability of the power-on charging scheme in Fig. 5 under various temperatures are plotted in Fig. 6(a), which can be defined as a product of the measurement probabilities of all rounds $P_g = \prod_m P_g(m)$. For charging the battery at the vacuum state, the success probability decreases with a very small rate. It is still over 93% when $m = 80$. For charging a finite-temperature thermal state, the success probability experiences an obvious decay during the first several ($m \approx 20$) rounds of measurements. Then the population distribution of battery is transformed to be a near-Gaussian one [see Figs. 5(b) and 5(c)] and it becomes sharper as the measurements are constantly implemented. It gives rise to $P_g(60 \leq m \leq 20) \approx 1$ and thus P_g is almost invariant before the occurrence of population inversion ($m \approx 60$). For a moderate temperature $\beta = 0.1/\omega_c$, the battery would be successfully charged with a 28% probability under $m = 80$ measurements. For the higher-temperature case $\beta = 0.03/\omega_c$, the success probability declines from 20% to 5% as $m = 60 \rightarrow m = 80$. During that period, the upperbound level- N is populated and then a significant portion of the near-Gaussian distribution of population has to be abandoned under normalization as more measurements are performed. It is thus expected to have a decreasing $P_g(m > 60)$.

The charging power defined in Eq. (11) can be observed in Fig. 6(b), also exhibiting a similar monotonic pattern under various temperatures in a large regime. The average population increases linearly with the measurement number and the optimized measurement interval is inversely proportional to the square root of the average population according to Eqs. (14) and (10), respectively. Then it is found that the charging power approximately increases as $\mathcal{P}(m) \propto \sqrt{\bar{n}^{(m)}}$. As also shown in Fig. 6(b), a higher temperature gives rise to a larger $\mathcal{P}(m)$ until a decline behavior after $m = 60$ measurements (see the green dot-dashed line). That is also induced by the population inversion, by which the average population of the battery fails to keep a linear increase as indicated by the green dotted line in Fig. 5(d).

IV. POWER-OFF CHARGING

When the measurement basis does not commute with the system Hamiltonian, energy is allowed to be taken away from the measurement apparatus and inserted to the system. In such a way, it turns to be useful work [26]. This section is devoted to analyse the power-off charging scheme described by \mathcal{M}_{ge} , in which charger qubits are prepared in their ground state with $q = 1$, and projective measurement is performed on the excited state with $\theta = \pi$ (see the upper right corner in Fig. 2). In this case, the energy variation in the charger-battery system is from the measurements alone. The battery state after m rounds of power-off charging reads

$$\rho_{\text{off}}^{(m)} = \frac{\mathcal{M}_{ge}[\rho_{\text{off}}^{(m-1)}]}{P_e(m)} = \frac{\sum_{n=0}^{N-1} |\lambda_{n+1}(\tau)|^2 p_{n+1}^{(m-1)} |n\rangle\langle n|}{P_e(m)}, \quad (18)$$

where $P_e(m) = \sum_{n=0}^{N-1} |\lambda_{n+1}(\tau)|^2 p_{n+1}^{(m-1)}$ is the measurement probability of the m th round. Equation (18) indicates that POVM \mathcal{M}_{ge} replaces the populations on low-energy states with that on their neighboring high-energy states with a τ -dependent factor $p_n^{(m)} \leftarrow |\lambda_{n+1}(\tau)|^2 p_{n+1}^{(m-1)}$. For a battery initially in a Gibbs state, whose population is maximized on the ground state, \mathcal{M}_{ge} could induce a certain amount of charging effect on the battery after population renormalization by moving a smaller occupation on higher levels to lower levels. However, in sharp contrast to \mathcal{M}_{eg} described by Eq. (8), here the low-energy states are always populated during the transfer from a thermal distribution to a near-Gaussian distribution.

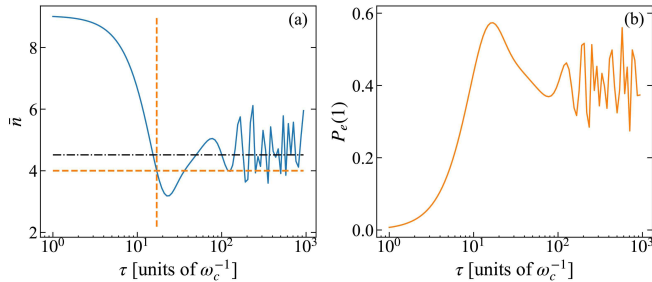


FIG. 7. (a) Average population and (b) Measurement probability as functions of measurement interval τ after a single measurement within the power-off scheme. In (a) the two crossing orange dashed lines locate the average population after a single measurement with a maximal measurement probability obtained from (b), which is found to be smaller than \bar{n}_{th} (denoted by the black dot-dashed line) in magnitude. It is then hard to keep charging the battery with a significant probability. Parameters are the same as those in Fig. 3.

The limited charging effect by the power-off scheme can be uncovered on the optimization of measurement intervals. We provide the average population of battery and the measurement probability under a single POVM \mathcal{M}_{ge} as functions of the measurement interval in Fig. 7(a)

and 7(b), respectively. Both of them present similar patterns as those under the power-on scheme in Fig. 3. However, it is found that the mean value of the population \bar{n} is less than its initial value \bar{n}_{th} (indicated by the black dot-dashed line) when τ is chosen such that the measurement probability attains the peak value. In this case, the battery is discharged rather than charged. In general, it is hard to charge the battery with a significant success probability under a number of rounds of evolution-and-measurement. In simulation of the power-off charging scheme, a compromise between the charging ratio of neighboring rounds $r = \bar{n}^{(m+1)}/\bar{n}^{(m)}$ and the success probability $P_e = \prod_m P_e(m)$ has to be made to optimize measurement intervals. Nevertheless, a not-too-small success probability constrains the measurement number in terms of an efficient charging-by-measurement scheme.

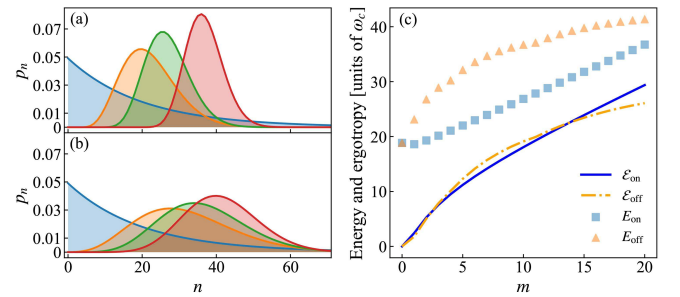


FIG. 8. Population distributions of the battery under (a) power-on and (b) power-off charging schemes after $m = 0$ (blue), $m = 5$ (orange), $m = 10$ (green), and $m = 20$ (red) measurements for $\beta = 0.05/\omega_c$. In (c), battery ergotropy and energy for two schemes are respectively plotted with lines and markers. The other parameters are the same as those in Fig. 3.

We now compare the charging efficiency under the power-on and power-off schemes. Their evolutions of the battery-population distribution under various number of measurements are demonstrated in Fig. 8(a) and 8(b). With the same setting of parameters and initial thermal state, it is found that both average population and variance of the Gaussian-like distribution under the power-off charging are larger than those under the power-on charging. For example, when $m = 20$, $\bar{n}^{(m)}$ are found to be about 37 and 41 and $\Delta n^{(m)}$ are about 24 and 98 for power-on and power-off charging schemes, respectively. Then the distribution under power-off charging is much more extended than power-on charging.

Mean value and variance of the battery population are associated with the battery ergotropy and energy in Fig. 8(c), respectively. Similar to Eqs. (16) and (17), we have $E_{\text{off}}^{(m)} \equiv \text{Tr}[H_B \rho_{\text{off}}^{(m)}]$ and $\mathcal{E}_{\text{off}}^{(m)} \equiv E_{\text{off}}^{(m)} - \text{Tr}[\sigma_{\rho_{\text{off}}^{(m)}} H_B]$ for the power-off scheme, where $\sigma_{\rho_{\text{off}}^{(m)}}$ is the passive state for $\rho_{\text{off}}^{(m)}$. For the power-off charging scheme, the battery cannot obtain energy from both charger qubits and the external energy input. It could be constantly charged by

projective measurements as indicated by p_n in Fig. 8(b) and E_{off} in Fig. 8(c). The charger qubit is also charged since the measurement is performed on excited state. In regard to the initial state of the charger qubits, the power-off charging scheme still converts initial thermal state of zero ergotropy to a high-ergotropy state, especially with less measurements (see $m = 5 \rightarrow m = 10$ in the yellow dot-dashed line). The numerical simulation at $m = 20$ shows that the success probabilities for the power-off and power-on schemes are about 1% and 26%, respectively. For $m \approx 20$, the charged energy for the battery under the power-off scheme is larger than that under the power-on scheme. But the latter takes advantage in ergotropy, a more important indicator for a quantum battery. When $m > 15$, the advantage becomes more significant with respect to the ratio of ergotropy and energy.

V. CONCLUSION

In summary, we have established a charging-by-measurement framework on rounds of joint-evolution-and-partial-projection, in which the charger system is a sequence of disposable qubits. General POVMs on the quantum battery of finite levels can be induced from the exchange interaction between charger and battery and the projective measurement on a general state of charger qubit. They can yield either charging or discharging ef-

fect in various regimes of the parametric space. It is found that significant charging could occur when the qubit is prepared at the excited state and measured on the ground state or in the opposite situation. They are termed as power-on and power-off charging schemes. We find that the power-on charging scheme is the most efficient in charging energy, charging power, and ergotropy-energy rate. Using optimized measurement intervals, our measurement-based charging could transform the battery from a finite-temperature state to a population-inversion state holding a near-unit ergotropy-energy rate and a significant success probability. Within less number of measurements than the power-on scheme, the power-off charging scheme can be used to charge the battery and charger qubits without external energy input, although it is hard to survive more rounds of measurements with a finite probability. Our work demonstrates that quantum measurement could be a useful thermodynamical resource analogous to conventional heat or work reservoirs, serving as efficient fuels powering a charging scheme through a nonunitary procedure.

ACKNOWLEDGMENTS

We acknowledge financial support from the National Science Foundation of China (Grants No. 11974311 and No. U1801661).

-
- [1] G. M. Andolina, M. Keck, A. Mari, V. Giovannetti, and M. Polini, *Quantum versus classical many-body batteries*, *Phys. Rev. B* **99**, 205437 (2019).
 - [2] A. Levy, L. Diósi, and R. Kosloff, *Quantum flywheel*, *Phys. Rev. A* **93**, 052119 (2016).
 - [3] S. Julià-Farré, T. Salamon, A. Riera, M. N. Bera, and M. Lewenstein, *Bounds on the capacity and power of quantum batteries*, *Phys. Rev. Research* **2**, 023113 (2020).
 - [4] K. V. Hovhannisyán, M. Perarnau-Llobet, M. Huber, and A. Acín, *Entanglement generation is not necessary for optimal work extraction*, *Phys. Rev. Lett.* **111**, 240401 (2013).
 - [5] R. Alicki and M. Fannes, *Entanglement boost for extractable work from ensembles of quantum batteries*, *Phys. Rev. E* **87**, 042123 (2013).
 - [6] G. M. Andolina, M. Keck, A. Mari, M. Campisi, V. Giovannetti, and M. Polini, *Extractable work, the role of correlations, and asymptotic freedom in quantum batteries*, *Phys. Rev. Lett.* **122**, 047702 (2019).
 - [7] M. Horodecki and J. Oppenheim, *Fundamental limitations for quantum and nanoscale thermodynamics*, *Nat. Commun.* **4**, 2059 (2013).
 - [8] F. Campaioli, F. A. Pollock, F. C. Binder, L. Céleri, J. Goold, S. Vinjanampathy, and K. Modi, *Enhancing the charging power of quantum batteries*, *Phys. Rev. Lett.* **118**, 150601 (2017).
 - [9] J.-Y. Gyhm, D. Šafránek, and D. Rosa, *Quantum charging advantage cannot be extensive without global operations*, *Phys. Rev. Lett.* **128**, 140501 (2022).
 - [10] F. Barra, *Dissipative charging of a quantum battery*, *Phys. Rev. Lett.* **122**, 210601 (2019).
 - [11] K. V. Hovhannisyán, F. Barra, and A. Imparato, *Charging assisted by thermalization*, *Phys. Rev. Research* **2**, 033413 (2020).
 - [12] G. M. Andolina, D. Farina, A. Mari, V. Pellegrini, V. Giovannetti, and M. Polini, *Charger-mediated energy transfer in exactly solvable models for quantum batteries*, *Phys. Rev. B* **98**, 205423 (2018).
 - [13] S. Seah, M. Perarnau-Llobet, G. Haack, N. Brunner, and S. Nimmrichter, *Quantum speed-up in collisional battery charging*, *Phys. Rev. Lett.* **127**, 100601 (2021).
 - [14] D. Ferraro, M. Campisi, G. M. Andolina, V. Pellegrini, and M. Polini, *High-power collective charging of a solid-state quantum battery*, *Phys. Rev. Lett.* **120**, 117702 (2018).
 - [15] F. C. Binder, S. Vinjanampathy, K. Modi, and J. Goold, *Quantacell: powerful charging of quantum batteries*, *New J. Phys.* **17**, 075015 (2015).
 - [16] T. P. Le, J. Levinsen, K. Modi, M. M. Parish, and F. A. Pollock, *Spin-chain model of a many-body quantum battery*, *Phys. Rev. A* **97**, 022106 (2018).
 - [17] D. Rossini, G. M. Andolina, and M. Polini, *Many-body localized quantum batteries*, *Phys. Rev. B* **100**, 115142 (2019).

- [18] D. Rossini, G. M. Andolina, D. Rosa, M. Carrega, and M. Polini, *Quantum advantage in the charging process of sachdev-ye-kitaev batteries*, *Phys. Rev. Lett.* **125**, 236402 (2020).
- [19] L. P. García-Pintos, A. Hamma, and A. del Campo, *Fluctuations in extractable work bound the charging power of quantum batteries*, *Phys. Rev. Lett.* **125**, 040601 (2020).
- [20] F. Caravelli, G. Coulter-De Wit, L. P. García-Pintos, and A. Hamma, *Random quantum batteries*, *Phys. Rev. Research* **2**, 023095 (2020).
- [21] B. Misra and E. C. G. Sudarshan, *The zeno's paradox in quantum theory*, *J. Math. Phys.* **18**, 756 (1977).
- [22] D. Home and M. Whitaker, *A conceptual analysis of quantum zeno; paradox, measurement, and experiment*, *Ann. Phys. (N.Y.)* **258**, 237 (1997).
- [23] P. Facchi and S. Pascazio, *Quantum zeno subspaces*, *Phys. Rev. Lett.* **89**, 080401 (2002).
- [24] C. Elouard, D. A. Herrera-Martí, M. Clusel, and A. Auffèves, *The role of quantum measurement in stochastic thermodynamics*, *npj Quantum Inf.* **3**, 9 (2017).
- [25] L. Buffoni, A. Solfanelli, P. Verrucchi, A. Cucoli, and M. Campisi, *Quantum measurement cooling*, *Phys. Rev. Lett.* **122**, 070603 (2019).
- [26] C. Elouard and A. N. Jordan, *Efficient quantum measurement engines*, *Phys. Rev. Lett.* **120**, 260601 (2018).
- [27] J.-s. Yan and J. Jing, *Simultaneous cooling by measuring one ancillary system*, *Phys. Rev. A* **105**, 052607 (2022).
- [28] H. Nakazato, T. Takazawa, and K. Yuasa, *Purification through zeno-like measurements*, *Phys. Rev. Lett.* **90**, 060401 (2003).
- [29] Y. Li, L.-A. Wu, Y.-D. Wang, and L.-P. Yang, *Non-deterministic ultrafast ground-state cooling of a mechanical resonator*, *Phys. Rev. B* **84**, 094502 (2011).
- [30] J.-S. Xu, M.-H. Yung, X.-Y. Xu, S. Boixo, Z.-W. Zhou, C.-F. Li, A. Aspuru-Guzik, and G.-C. Guo, *Demon-like algorithmic quantum cooling and its realization with quantum optics*, *Nat. Photonics* **8**, 113 (2014).
- [31] C. M. Caves, *Quantum mechanics of measurements distributed in time. a path-integral formulation*, *Phys. Rev. D* **33**, 1643 (1986).
- [32] C. M. Caves and G. J. Milburn, *Quantum-mechanical model for continuous position measurements*, *Phys. Rev. A* **36**, 5543 (1987).
- [33] R. Kosloff, *Quantum thermodynamics and open-systems modeling*, *J. Chem. Phys.* **150**, 204105 (2019).
- [34] V. Paulsen, *Completely Bounded Maps and Operator Algebras* (Cambridge University Press, Cambridge, 2003).
- [35] A. E. Allahverdyan, R. Balian, and T. M. Nieuwenhuizen, *Maximal work extraction from finite quantum systems*, *Europhys. Lett.* **67**, 565 (2004).
- [36] U. Fano, *Ionization yield of radiations. ii. the fluctuations of the number of ions*, *Phys. Rev.* **72**, 26 (1947).